First-principles calculations of x-ray absorption near edge structure and energy loss near edge structure: present and future

2009 J. Phys.: Condens. Matter 21 104201

(http://iopscience.iop.org/0953-8984/21/10/104201)

IOP PUBLISHING JOURNAL OF PHYSICS: CONDENSED MATTER

J. Phys.: Condens. Matter **21** (2009) 104201 (9pp) doi:10.1088/0953-8984/21/10/104201

First-principles calculations of x-ray absorption near edge structure and energy loss near edge structure: present and future

Isao Tanaka[1,2] **and Teruyasu Mizoguchi**[3]

[1] Department of Materials Science and Engineering, Kyoto University, Sakyo, Kyoto 606-8501, Japan
[2] Nanostructures Research Laboratory, Japan Fine Ceramics Center, Atsuta, Nagoya 456-8587, Japan
[3] Institute of Engineering Innovation, The University of Tokyo, Yayoi, Bunkyo, Tokyo 113-8656, Japan

E-mail: tanaka@cms.MTL.kyoto-u.ac.jp

Received 17 October 2008
Published 10 February 2009
Online at stacks.iop.org/JPhysCM/21/104201

Abstract

Computational methods for theoretical x-ray absorption near edge structure (XANES) and energy loss near edge structure (ELNES) are classified into a few groups. Depending on the absorption (or excitation) edge, required accuracy and desired information, one needs to select the most suitable method. In this paper, after providing a map of available computational methods, some examples of first-principles calculations of XANES/ELNES for selected wide gap materials are given together with references. For ZnO, for example, experimental spectra at three edges, Zn K, L_3, and O K, including their orientation dependence, are well reproduced by the supercell calculations with a core hole. Good agreement between theoretical and experimental spectra of ZnO alloys can also be seen. *Theoretical fingerprints* are satisfactorily obtained in this way. However, there are remaining issues beyond 'good agreements' which need to be solved in the future.

(Some figures in this article are in colour only in the electronic version)

1. Introduction

XANES stands for x-ray absorption near edge structure, which corresponds to the first 30–50 eV of XAFS (x-ray absorption fine structure) from the x-ray absorption edge. NEXAFS (near edge XAFS) is a synonym for XANES. The rest of the spectrum is called the EXAFS (extended XAFS). A typical experimental XAFS is shown in figure 1. Both XANES and EXAFS are sensitive to the local environment of excited atoms, and they provide complementary information. The former is sensitive to the properties of the chemical environment of the specific element: chemical bonding, charge state, magnetic state etc [1–3]. On the other hand, EXAFS can reveal properties of the local coordination of the atom, such as coordination number and bond length, quantitatively [4]. The recent development of a third-generation synchrotron source has enabled the measurement of XANES of trace elements to a ppm level when combined with the use of highly efficient detectors [5, 6].

ELNES is the acronym for electron energy loss near edge structure, which corresponds to the low energy portion of the EELS (electron energy loss spectrum) in the core loss region [7–10]. A modern TEM (transmission electron microscope) is often equipped with an EELS detector. Employing a TEM or scanning TEM dedicated to high spatial resolution study, one can obtain ELNES from the sub-nanometer region [11–13]. Information that can be obtained from ELNES is almost identical to that from XANES when the ELNES is measured with transmission geometry. ELNES has the advantage of allowing analyzing absorption edges that

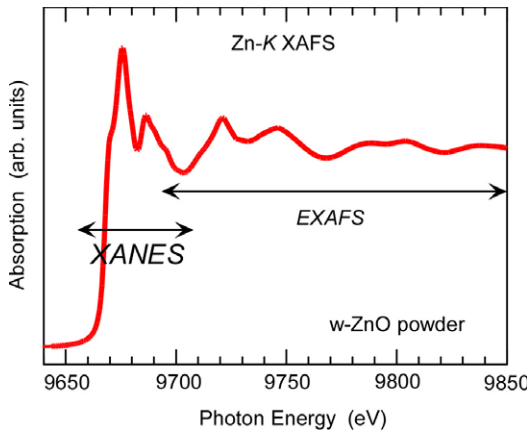

Figure 1. Experimental Zn K XAFS of w-ZnO.

are lower than 2 keV, which correspond to K edges of light elements up to Si, and L edges up to fourth-row elements in the periodic table, which includes 3d transition elements. On the other hand, XANES can be used for investigating most of the elements in the periodic table even at the K edge. As a trade-off with the high special resolution, one must pay attention to minimizing the irradiation damage caused by focusing of the electron beam on the ELNES measurement. An x-ray beam, however, typically cannot be focused down to a nanosized area. XANES and ELNES are therefore complementary techniques.

Interpretation of experimental XANES/ELNES has been effected via a fingerprinting technique. Traditionally, experimental spectra of reference compounds were used to identify the local environment of a specific element in a sample. However, there are obvious limitations in the fingerprinting technique, on the basis of the experimental spectra. It can be applied only when the database of reference compounds is complete. We are often interested in the analysis of new or exotic compounds, surface, interface and lattice imperfections, etc. Then reference spectra are hard to find. We therefore need a good theoretical tool for producing reliable theoretical spectra, which can be used as references for the fingerprinting technique. Historically a number of techniques with a wide variety of approximations have been used to obtain *theoretical fingerprints*. Some methods that were prohibitively expensive in the past can now be used because of developments of high performance computers and numerical techniques. First-principles calculations for complex systems composed of 100–1000 atoms are already in practical use. There are a few techniques that can treat correlations among multi-electrons explicitly beyond the one-electron theory when necessary. From an experimentalist viewpoint, one needs to find guidance for selecting the most suitable method for interpreting the spectra. The method should be chosen according to the absorption (or excitation) edge, required accuracy and desired information. In this paper, after providing a map of theoretical methods in the second section, some examples of first-principles calculations of XANES/ELNES for selected wide gap materials are given, together with references in the third section. In the fourth section, we point out remaining issues beyond 'good agreements', which need to be solved in the future.

2. Principles and classification of XANES and ELNES calculations

Both XANES and ELNES reflect the electronic transition from a core level to unoccupied states. The photo-absorption coefficient, μ, or photo-absorption cross section (PACS) can be generally described using Fermi's golden rule as

$$\mu \propto \sum_f |\langle\psi_\mathrm{f}| \exp(\mathrm{i}\boldsymbol{kr}) \cdot \boldsymbol{e} \cdot \boldsymbol{P}|\psi_\mathrm{i}\rangle|^2 \delta(\hbar\omega - E_\mathrm{f} + E_\mathrm{i}) \quad (1)$$

where ψ_f and ψ_i are multi-electron wavefunctions at the final state and initial state, respectively. E_f and E_i are total energies of the corresponding states. $\hbar\omega$, $\boldsymbol{k}$ and $\boldsymbol{e}$ are the energy, the wavenumber vector and the unit vector for the polarization direction of the x-rays. $\boldsymbol{P}$ is the sum of the linear momentum operators of the electrons. In the XAS, because $\boldsymbol{kr} \ll 1$ and $\exp(\mathrm{i}\boldsymbol{kr}) \approx 1$, the equation can be approximated using one-electron wavefunctions of the core state ϕ_i, and that of the excited electron, ϕ_f, as

$$\mu \propto \sum_f |\langle\phi_\mathrm{f}|\boldsymbol{e} \cdot \boldsymbol{r}|\phi_\mathrm{i}\rangle|^2 \delta(\hbar\omega - E_\mathrm{f} + E_\mathrm{i}) \quad (2)$$

where $\boldsymbol{r}$ is the position of the excited electron. This corresponds to the electric dipole transition.

The intensity of the ELNES within the dipole approximation can be described by

$$I \propto \sum_f |\langle\phi_\mathrm{f}|\boldsymbol{q} \cdot \boldsymbol{r}|\phi_\mathrm{i}\rangle|^2 \delta(\hbar\omega - E_\mathrm{f} + E_\mathrm{i}) \quad (3)$$

where $\boldsymbol{q}$ is the scattering vector or momentum transfer of the incident electron. $\hbar\omega$ is the electron energy loss in this case. As can be understood from the analogy of equations (2) and (3), the scattering vector $\boldsymbol{q}$ for ELNES plays the same role as the polarization vector $\boldsymbol{e}$ in XANES. The two spectra are comparable and the computational procedures for obtaining the theoretical spectra are therefore identical.

A number of theoretical methods have been used to obtain theoretical XANES/ELNES. Table 1 summarizes the methods available in recent years. Band structure calculation on the basis of the density functional theory (DFT) is one of the most popular methods [14–18]. It should be emphasized that in the early days calculations often ignored the electronic relaxation associated with the presence of the core hole at the final state and additional correlation between the core hole and the excited electron. In other words, the core hole effects were ignored. Such calculations failed to reproduce the experimental spectra. Recently there has been a consensus that the proper inclusion of the core hole effect is mandatory for the reproduction of XANES/ELNES for wide gap materials using band structure calculations. The squares of the wavefunctions located at the bottom of the unoccupied band of rocksalt MgO (RS-MgO) plotted on a (100) plane for a ground state and for a final state of Mg K and Mg $L_{2,3}$ x-ray absorptions are compared in figure 2. Calculations of the final states were made with a supercell composed of 128 atoms. The wavefunction at the bottom of the unoccupied band of MgO is mainly of Mg 3s type, periodically arrayed at the ground state. When

Table 1. Classification of modern methods of computation for theoretical XANES/ELNES.

(1) Supercell DFT calculations with a core hole Band structure methods have been widely used for studying theoretical K edge XANES/ELNES and other edges except for transition elements having open d and f shells. Supercells exceeding 100 atoms are typically required and the effect of the core hole should be included in the self-consistent calculation. The core hole can be included for all electron methods in a straightforward manner. The theoretical transition energy can be computed as the difference in total energy between final and initial states. When core orbitals are eliminated in the ground state calculations, such as in cases of pseudopotentials or frozen core methods, special attention should be paid to maintaining the accuracy of the final state calculations.
(2) Multiple-scattering (MS) calculations using model clusters A unique method for reproducing XANES/ELNES in an extended energy range. Calculations on model clusters composed of a few tens to hundreds of atoms have been satisfactorily used for many systems excluding transition elements having open d and f shells. The dependence/convergence of theoretical spectra in relation to the cluster size and shape, number of scattered waves, degrees of approximation (full potentials or not) etc should be carefully examined.
(3) Bethe–Salpeter equation (BSE) calculations using primitive cells By solving the Bethe–Salpeter equation (BSE), bound exciton states which form due to the Coulomb interaction between the excited electron and the positively charged hole can be obtained by calculation. Sharp excitonic features can be found in experimental XANES/ELNES of wide gap materials when they are measured at shallow core edges with high energy resolution. Although full BSE calculations within all electron schemes are computationally very demanding, some successes in reproducing the XANES/ELNES at shallow edges have been demonstrated recently.
(4) Multiplet calculations using model clusters Widely spread multiplet structures appear in the $L_{2,3}$ XANES/ELNES of 3d transition metal compounds having an open 3d shell because of the strong correlation among electrons and that between the core holes. The same is true for rare-earth compounds with an open 4f shell. Either semi-empirical charge transfer multiplet calculations or *ab-initio* CI calculations using molecular orbitals can be used to compute the multiplet structures. They have satisfactorily reproduced spectra of many compounds having different d or f electron numbers and coordination numbers using model clusters. However, such calculations are still limited to model clusters with a single metal ion because of the large computational demand.

the core hole is produced, one can find clear localization of the wavefunction near the excited Mg atom with a small contribution from the neighboring O 2p. The magnitude of the localization is more significant for the Mg 1s hole as compared to the Mg 2p hole. The strategy for computing for the excited atom under periodic boundary conditions is analogous to that of impurity calculations. If the size of the periodic unit, i.e., the supercell, is too small, artificial interaction between excited atoms overwhelms the results. In order to reduce such interactions, one has to carefully choose a large supercell. In our experience, a typical supercell size of greater than 1 nm, which usually includes approximately 100 atoms, is required to see the convergence of the spectral shape, although the optimum cell size should depend on the electronic structure of the material of interest. The core hole can be included in a straightforward manner for all electron calculations. On the other hand, core orbitals are eliminated from the final secular equation in the other type of calculation. In order to include a core hole in such calculations, special treatments such as generation of excited pseudopotentials [17] or the switching of semi-core orbitals to core orbitals [16] are required. Special attention should be paid to maintaining the accuracy in such cases.

Band structure calculations using supercells composed of more than 100 atoms became practical only recently. Before that, a number of trials aiming to reproduce XANES/ELNES had been attempted. One of the most successful approaches in the past was via first-principles cluster calculations. Because the wavefunction of the excited electron is localized anyway due to the presence of the core hole, calculations using small clusters can reproduce the major features of experimental spectra [19–25].

The other major method is called the multiple-scattering approach, which computes the scattering phenomena for the excited electron associated with the absorption or excitation. This approach is a standard technique for analyzing EXAFS that appears well above the absorption edge. Since XANES and EXAFS can be treated within the same theoretical framework by varying the energy of the excited electron, it is quite natural that the multiple-scattering method has been a popular approach especially for x-ray spectroscopists. Recent progress with this method can be found elsewhere [26–29].

Use of a reliable band structure calculation and a large supercell with inclusion of a core hole is one of standard methods for theoretical XANES/ELNES studies of wide gap materials. Most of the K edge XANES/ELNES can be reasonably well reproduced in this way. However, the strong correlation among electrons and that between the core hole and the excited electron totally change the spectral shape when the atomic orbital of the excited electron is spatially localized as in the case of 3d orbitals for transition metal compounds and 4f orbitals for rare-earth compounds. The 3d orbital can be monitored via $L_{2,3}$ edge spectra in which the 2p $\rightarrow$ 3d transition is predominant. The 3d electrons show widely spread multiplet structures because of the strong electronic correlation. The presence of the 2p core hole introduces further complexity into the spectra. This type of calculation was possible in the past only by using an empirical approach involving a number of semi-empirical parameters, as reviewed in the reference [30]. Recently, electronic correlations among 3d electrons and a 2p hole were rigorously calculated in a first-principles manner by taking all Slater determinants produced from molecular orbitals. In the quantum chemistry terminology, this is the configuration interaction (CI) calculation using molecular orbitals via DFT calculations, namely the *ab-initio* CI method. Experimental spectra from many compounds having different d electron

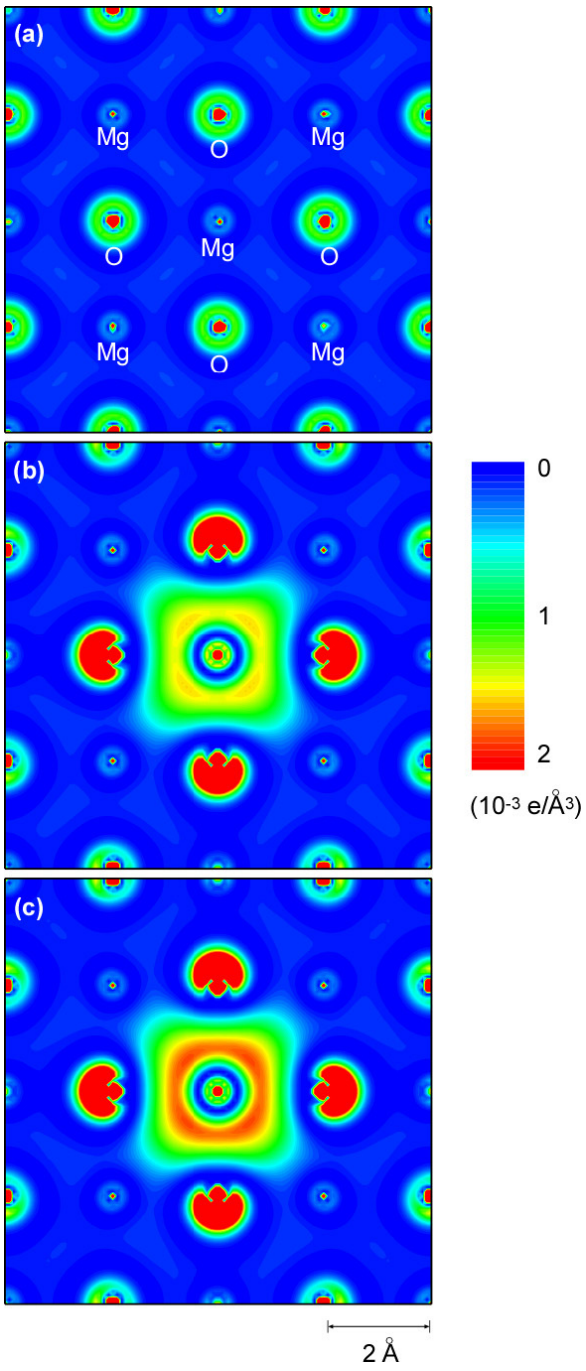

Figure 2. The squares of the wavefunctions located at the bottom of the conduction band of the MgO(001) plane for a 128-atom supercell (a) without a core hole (ground state), (b) with a Mg 2p hole, and (c) with a Mg 1s hole.

numbers and coordination numbers have been successfully reproduced [31–36]. A review of multiplet calculations can be found elsewhere [37, 38].

A sharp excitonic feature is often found in experimental XANES/ELNES when they are measured with high energy resolution. The bound exciton states can form due to the Coulomb interaction between the excited electron and the positively charged hole. Since the standard DFT method treats the electron and the hole as independent, it cannot calculate the excitonic states. The correlation between the core hole and the excited electron can be explicitly treated using the two-particle Green's function by solving the Bethe–Salpeter equation (BSE) [39–41]. Although full BSE calculations within all electron schemes are computationally very demanding, some successes in reproducing the XANES/ELNES at shallow edges have been demonstrated recently [42, 43]. The sharp excitonic feature is smeared out when the energy resolution is low. Recently the experimental energy resolution has been getting much better, especially for ELNES, with the development of electron beam monochromators. There will be more demands for such BSE calculations for reproducing the excitonic features which were hidden before. This should be even more important for wide gap materials when monitored at the shallow core XANES/ELNES.

3. Supercell DFT calculations with a core hole

Theoretical XANES/ELNES have been reported by the group of the present authors for a number of wide gap materials including TiO_2, $SrTiO_3$, $BaTiO_3$, AlN, GaN, InN, ZnO and their polymorphs [3, 15, 44, 45]. Dilute Mn dopant in w-ZnO [46], solid solutions of β-SiAlON [47], ZnO–Al_2O_3 [48] and MgO–ZnO [49] were investigated as well. The crystallographic orientation dependences of the spectra were also examined. As a set of examples of such calculations, results for ZnO and its alloy are shown in this section. It is also worth referring to the review paper by Hébert [16] on the ELNES calculations by the F(L)APW + lo method using the WIEN2k code [50]. Another review for theoretical calculations of ELNES was published very recently [51]. Some examples were shown there together with many references.

All calculations shown in this paper were made by the orthogonalized linear combinations of atomic orbitals (OLCAO) method developed by Ching *et al* [14, 18, 52]. This is a first-principles band structure method based on DFT with the local density approximation (LDA). Each atomic orbital is expressed as a sum of Gaussian-type orbitals. Separate calculations at a ground state and an excited state were made. The photo-absorption coefficient was computed according to equation (2). The photo-absorption coefficient was typically convoluted with a Gaussian function of 1.0 eV FWHM. The theoretical transition energy was evaluated by the subtraction of the total energy at the ground (initial) state from that at the final state. Unless otherwise noted, theoretical spectra for non-cubic crystals were averaged over crystallographic orientations.

ZnO transforms to a rocksalt structure under high pressures. It also exhibits metastable zinc-blende structure under appropriate growth conditions. The major structural difference between wurtzite and zinc-blende structure is in the layer stacking sequence along the [001] direction. The point symmetry of the tetrahedral unit [ZnO_4] is also different. [ZnO_4] in the wurtzite structure has a C_{3v} symmetry which has lower symmetry than the zinc-blende structure, T_d. The coordination number of all atoms in the two phases is 4, whereas it is 6 in the rocksalt phase. Figure 3 summarizes all experimental and theoretical results for three

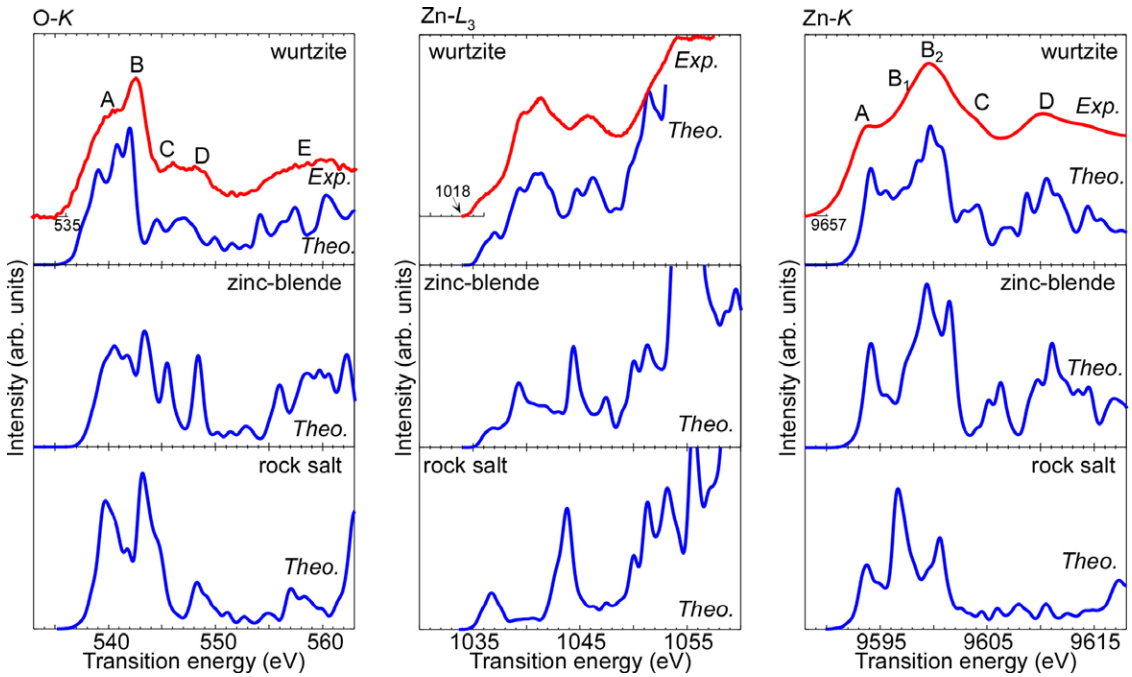

Figure 3. Theoretical XANES of three ZnO polymorphs at three different edges. They are compared to experimental spectra for the wurtzite phase.

polymorphs of ZnO at three different edges. Theoretical spectra for the wurtzite, zinc-blende and rocksalt phases were obtained using 108-, 128- and 128-atom supercells, respectively. Complete experimental data are available only for the wurtzite structure [15]; these are well reproduced by the computation. The Zn K XANES of rocksalt $Zn_{0.85}Mg_{0.15}O$ thin film synthesized by the pulsed laser deposition (PLD) technique on an MgO substrate was reported [53]. The experimental XANES of the film showed good agreement with the theoretical one.

In non-cubic systems, the orientation dependence of XANES/ELNES provides valuable information on anisotropic properties of crystals. Figure 4 shows results for w-ZnO, which has a hexagonal lattice. The experimental XANES was obtained using polarized x-rays for which the electric field, $\boldsymbol{E}$, is either parallel or perpendicular to the c-axis of the (0001) oriented ZnO thin film, as denoted by $\boldsymbol{c} \parallel \boldsymbol{E}$ and $\boldsymbol{c} \perp \boldsymbol{E}$, respectively [15, 54]. Theoretical spectra were obtained using equation (2) within the dipole approximation using the OLCAO method. The average of two spectra, i.e., $[(2/3)(\boldsymbol{c} \perp \boldsymbol{E}) + (1/3)(\boldsymbol{c} \parallel \boldsymbol{E})]$, corresponds to the spectrum that can be obtained from a powder sample (as in figure 3). It can be noted that peaks B_1 and C in the Zn K XANES are mainly composed of $\boldsymbol{c} \parallel \boldsymbol{E}$ components, whereas peak B_2 is composed of the $\boldsymbol{c} \perp \boldsymbol{E}$ component. Clear crystallographic dependence can also be predicted for the O K XANES. Contrary to the case for K XANES, the anisotropy of the spectra is small for the Zn L_3 XANES. This can be ascribed to different atomic orbitals that are responsible for K and L_3 XANES. The first few eV of the Zn K edge reflect mainly 4p-type orbitals, while the first few eV of the Zn L_3 XANES reflect mainly 4s orbitals. The spherical nature of the 4s orbital is the reason for the weaker dependence of the L_3 XANES on the orientation. Orientation dependence of the theoretical XANES was used to identify nanotexture of wurtzite AlN thin films deposited by the PLD technique [55].

XANES/ELNES is used to investigate the local environment of alloying elements. When the dopant is dilute and isolated, the theoretical spectrum can be obtained in the same way as that for the undoped crystals using a supercell model. The Zn K XANES of 30 ppm Zn in MgO [5] and the Mn K XANES of 5% Mn in ZnO [46] are typical examples. For the concentrated alloys, theoretical calculations can be more complicated. A wide range of solid solutions are known to form in silicon nitride, Si_3N_4, via double substitution of Si by Al and N by O; the product is called sialon, with general chemical formula $Si_{6-z}Al_zO_zN_{8-z}$ ($0 \leqslant z \leqslant 3.8$ for the β-phase). Solute arrangements of β- and γ-phase sialons were identified from the Al K XANES and theoretical fingerprints of many different solute arrangements [47]. It was concluded that Al solutes are predominantly coordinated by O atoms forming nearest neighbor Al–O bonds. On the other hand, pseudobinary MgO–ZnO with a rocksalt structure is known to show a very weak tendency to ordering [49]. In order to calculate XANES of the disordered MgO–ZnO solid solution, we adopted the cluster expansion method [49]. Firstly, theoretical spectra were computed for six ordered structures. Then, the theoretical spectrum of a disordered structure was constructed as the weighted sum of XANES of the ordered structures, with weighting factors obtained by the cluster expansion method. Theoretical results were then compared with experimental ones at several concentrations. Figure 5 shows theoretical spectra of six ordered alloys with different alloy compositions. Experimental Zn L_3 XANES at five compositions can be satisfactorily compared with theoretical spectra obtained in this way, as shown in figure 6.

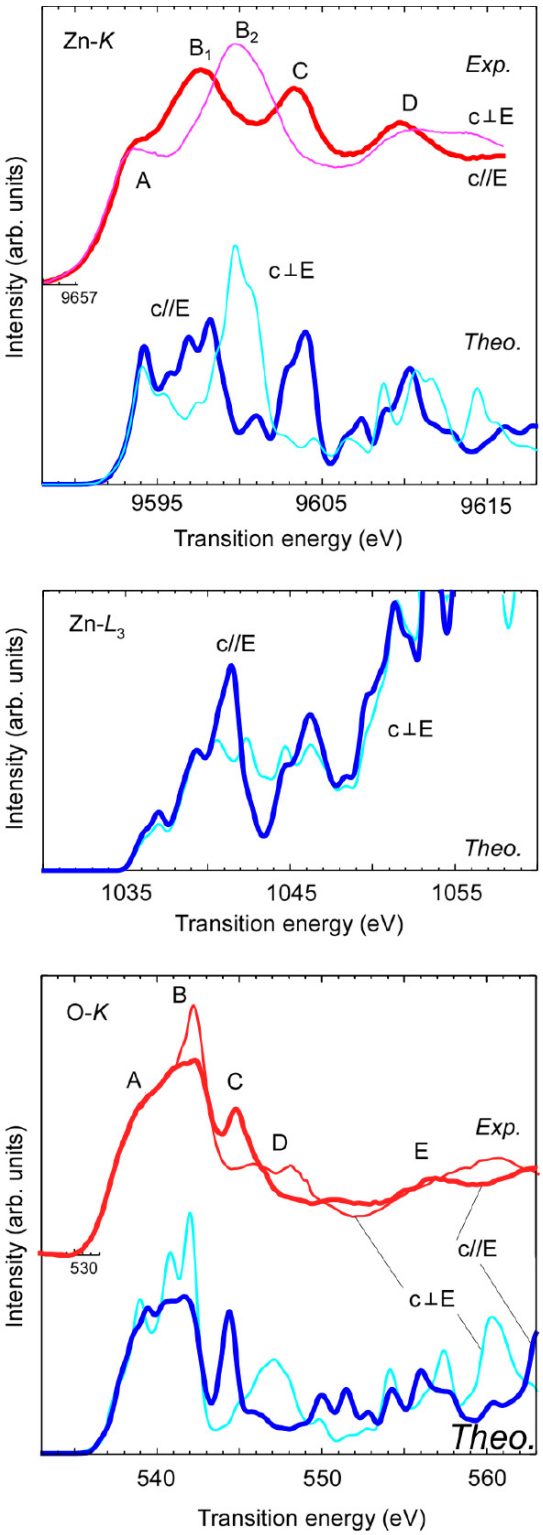

Figure 4. Orientation dependence of XANES from experiment and theory for w-ZnO at three different edges. The experimental O K XANES is obtained from [54].

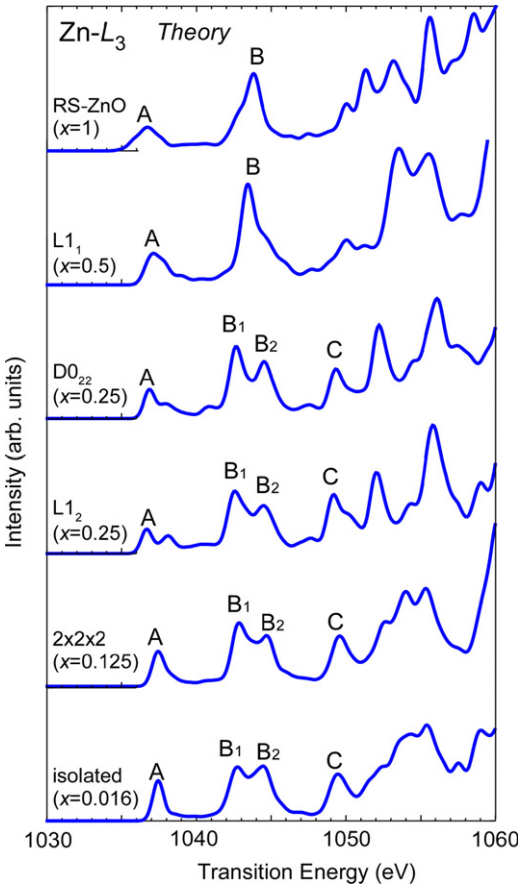

Figure 5. Theoretical Zn L_3 XANES of six ordered $Mg_{1-x}Zn_xO$ structures: i.e., RS-ZnO (RS: rocksalt; $x = 1$), $L1_1$ ($x = 0.5$), $D0_{22}$ ($x = 0.25$), $L1_2$ ($x = 0.25$), $2 \times 2 \times 2$ ($x = 0.125$), and the isolated Zn ($x = 0.016$) models.

4. Summary and prospects beyond 'good agreements'

Supercell DFT calculations with a core hole show 'good agreements' with experimental spectra in the region of 20–30 eV from the edge in wide gap materials. However, detailed examination finds some systematic inconsistencies between theory and experiment. The absolute theoretical transition energy obtained as the total energy difference between final and initial states usually differs from the experimental value by approximately 1% of the transition energy. The major source of the error may be the use of the one-electron theory [56]. If the error can be corrected just by a simple translation of the absolute energy scale, it does not cause a serious problem for the theoretical fingerprints. However, such errors sometimes change the appearance of the spectral shape. This happens when the sample contains multiple atomic sites with different local environments. In θ-Al_2O_3, for example, the crystal contains two kinds of Al sites, i.e., tetrahedrally (tet-Al) and octahedrally (oct-Al) coordinated ones with the number ratio of 1:1. In order to obtain theoretical Al K and $L_{2,3}$ XANES/ELNES of θ-Al_2O_3, a set of calculations for two sites should be made. Two spectra are then superposed with the weight of 1:1 to make the theoretical spectrum. Theoretical and experimental results for Al $L_{2,3}$ for θ-Al_2O_3 are shown in figure 7 [57, 58]. As can be seen, the peaks A and B originate from tet-Al and oct-Al, respectively. When the two spectra are properly superposed, the theoretical spectrum should reproduce the

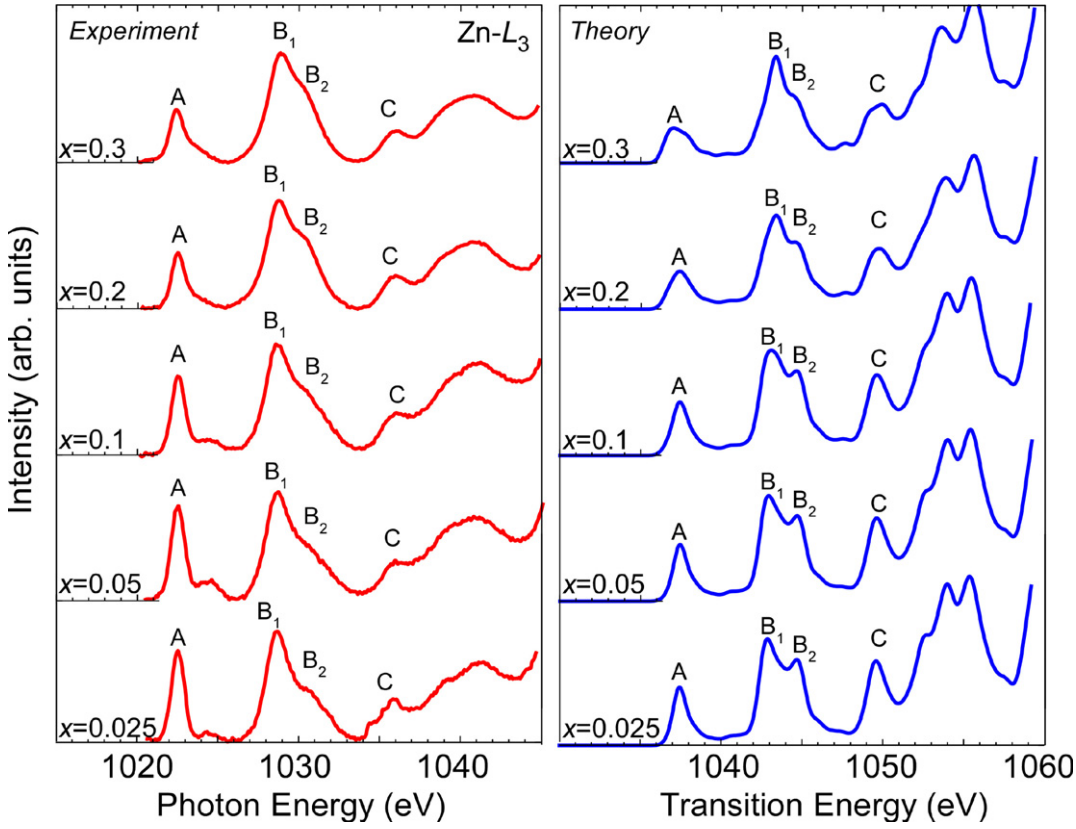

Figure 6. Left: experimental Zn L_3 XANES of five $Mg_{1-x}Zn_xO$ solid solutions with rocksalt structures. Right: theoretical spectra constructed as the weighted sum of theoretical XANES of the ordered structures with weighting factors obtained by the cluster expansion method.

experimental spectrum with a level of accuracy similar to that for a compound with a single Al site. The theoretical spectrum shown in figure 7 does not exhibit the problem. However, if a small error exceeding a few tenths of an eV occurs in the relative energy, between the spectra of two sites, the separation between peaks A and B is changed. Eventually, the appearance of the spectral shape becomes different.

Errors in relative energy make problems for identifying the chemical environment of elements which can be discussed through chemical shifts. Figure 8 shows experimental As K XANES of As_2O_3 and As_2O_5 crystals [59]. The chemical shift at the peak top is 5.0 eV. Theoretical spectra should have an accuracy to reproduce the chemical shift if one wants to discuss the chemical environment. Even when the formal charge of cations is the same, a clear chemical shift can be observed, for example, in the Al K XANES of w-AlN and α-Al_2O_3 [47]. Although the formal charge of Al is +3 for both of them, a shift by 4.1 eV at the first peak is observed. The shift can be well reproduced by the present calculation as shown in figure 9. These two examples together with many others should be used as benchmarks of the accuracy of the theoretical chemical shift. Systematic correction of errors in the energy scale associated with the DFT calculations should be solved in the future. A beyond LDA scheme such as the *GW* method may solve at least a part of the problem.

In this paper, we demonstrate that inclusion of a full core hole in a sufficiently large supercell gives a reasonable way to reproduce experimental spectra in wide gap materials. This

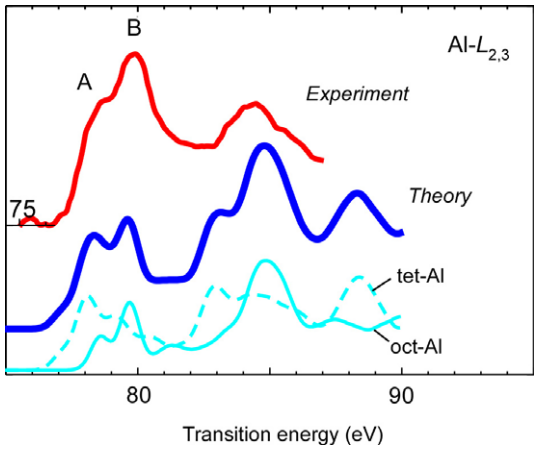

Figure 7. Experimental Al $L_{2,3}$ ELNES [58] for θ-Al_2O_3 in comparison to the theoretical one. θ-Al_2O_3 contains tetrahedrally (tet-Al) and octahedrally (oct-Al) coordinated Al with the number ratio of 1:1.

implies that the core hole remains almost unchanged during the excitation process in the insulators. On the other hand in metallic systems, the core hole is screened very effectively by the valence electrons. In this case, the introduction of a partial core hole or even complete disregard of the hole result in better reproduction of experimental spectra [16, 60, 61]. However, the magnitude of the partial hole should be dependent on the

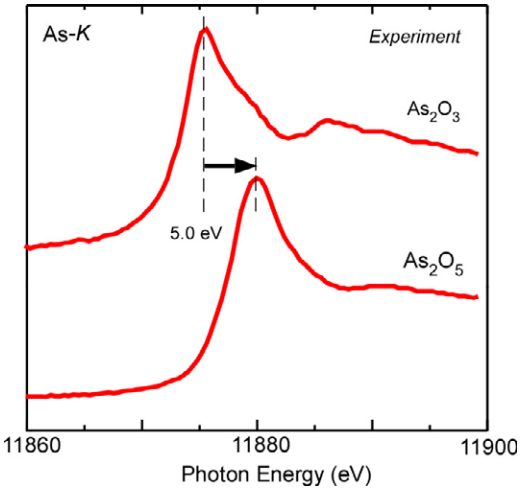

Figure 8. Experimental As K XANES of As_2O_3 and As_2O_5.

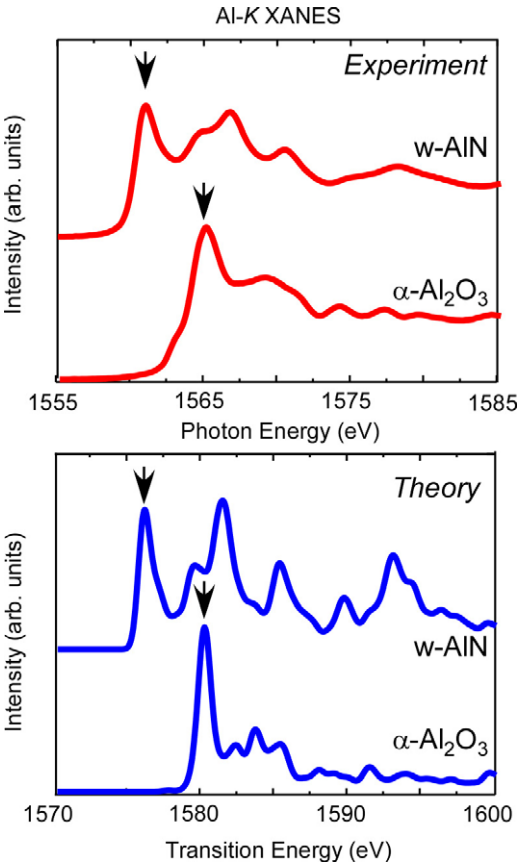

Figure 9. Comparison of Al K XANES of wurtzite AlN and corundum Al_2O_3 (α-Al_2O_3). Arrows indicate the peak positions for measuring the chemical shift. The top and bottom panels correspond to experimental and theoretical results, respectively.

electronic structure of the materials. It is indeed frustrating to include a partial core hole as an empirical parameter in otherwise first-principles calculations. In order to make more rigorous calculations, one has to go beyond the single-particle description and treat the electron–hole interactions within many body theory. The use of the Bethe–Salpeter equation (BSE) as described in the previous section should provide one straightforward way. Such calculations are still in the early stages.

Determination of the broadening width for theoretical XANES/ELNES is an important issue, to be solved in the future. In the present study, and in most of the other studies, Gaussians, Lorentzians, and their combinations with a fixed width are used to compare theoretical and experimental spectra. When the instrumental resolution is poor, this is a good approach since fine structures are anyway smeared out. It is not enjoyable to play with the selection of the broadening functions as kinds of fitting parameters. The experimental energy resolution has been getting better recently; it is approaching the intrinsic width of the spectra. There will be more demands for knowing the broadening width from theoretical calculations. A number of factors contribute to the broadening. Core hole lifetime broadening is one of the mechanisms. Data from both experimental analysis and atomic calculations can be found in the literature [2, 62, 63]. There are some other factors that we have to consider, such as the coupling of core transitions to phonons, the lifetime of an excited electron, and some dynamic effects among many electrons. Evaluation of broadening factors is still a problem for theoretical XANES/ELNES.

Acknowledgments

We are grateful to W Y Ching of the University of Missouri Kansas City for allowing us to use the OLCAO code and valuable discussion over a decade. This work is supported by a Grant-in-Aid for Scientific Research on Priority Areas 'Nano-Materials Science for Atomic Scale Modification 474' from the Ministry of Education, Culture, Sports, Science and Technology (MEXT) of Japan.

References

[1] Stöhr J 1992 *NEXAFS Spectroscopy* (Berlin: Springer)
[2] Fuggle J C and Inglesfield J E (ed) 1992 *Unoccupied Electronic States: Fundamentals for XANES, EELS, IPS and BIS* (*Springer Topics in Applied Physics*) (Berlin: Springer)
[3] Tanaka I, Mizoguchi T and Yamamoto T 2005 *J. Am. Ceram. Soc.* **88** 2013
[4] Lee P A, Citrin P H, Eisenberger P and Kincaid B M 1981 *Rev. Mod. Phys.* **53** 769
[5] Tanaka I, Mizoguchi T, Matsui M, Yoshioka S, Adachi H, Yamamoto T, Okajima T, Umesaki M, Chig W Y, Inoue Y, Mizuno M, Araki H and Shirai Y 2003 *Nat. Mater.* **2** 541
[6] Mizoguchi T, Sakurai M, Nakamura A, Matsunaga K, Tanaka I, Yamamoto T and Ikuhara Y 2004 *Phys. Rev.* B **70** 153101
[7] Egerton R F 1996 *Electron Energy-Loss Spectroscopy in the Electron Microscopy* (New York: Plenum)
[8] Ahn C C (ed) 2005 *Transmission Electron Energy Loss Spectrometry in Materials Science and the EELS Atlas* 2nd edn (New York: Wiley–VCH)
[9] Brydson R 2001 *Electron Energy Loss Spectroscopy* (Oxford: BIOS Scientific Publishers)
[10] Williams D B and Carter C B 2004 *Transmission Electron Microscopy: a Textbook for Materials Science* (Berlin: Springer)

[11] Varela M, Findlay S D, Lupini A R, Christen H M, Borisevich A Y, Dellby N, Krivanek O R, Nellist P D, Oxley M P, Allen L J and Pennycook S J 2004 *Phys. Rev. Lett.* **92** 95502
[12] Klie R F, Buban J P, Varela M, Franceschetti A, Jooss C, Zhu Y, Browning N D, Pantelides S T and Pennycook S J 2006 *Nature* **435** 475
[13] Mizoguchi T, Varela M, Buban J P, Yamamoto T and Ikuhara Y 2008 *Phys. Rev.* B **77** 024504
[14] Mo S D and Ching W Y 2000 *Phys. Rev.* B **62** 7901
[15] Mizoguchi T, Tanaka I, Yoshioka S, Kunisu M, Yamamoto T and Ching W Y 2004 *Phys. Rev.* B **70** 45103
[16] Hébert C 2007 *Micron* **38** 12
[17] Gao S P, Pickard C J, Payne M C, Zhu J and Yuan J 2008 *Phys. Rev.* B **77** 115122
[18] Ching W Y and Rulis P 2009 *J. Phys.: Condens. Matter* **21** 104202
[19] Tanaka I and Adachi H 1996 *Phys. Rev.* B **54** 4604
[20] Kanda H, Yoshiya M, Oba F, Ogasawara K, Adachi H and Tanaka I 1998 *Phys. Rev.* B **58** 96936
[21] Tanaka I, Araki H, Yoshiya M, Mizoguchi T, Oba F and Adachi H 1999 *Phys. Rev.* B **60** 4944
[22] Mizoguchi T, Tanaka I, Yoshiya M, Oba F, Ogasawara K and Adachi H 2000 *Phys. Rev.* B **61** 2180
[23] Mizoguchi T, Tanaka I, Yoshiya M, Oba F and Adachi H 1999 *J. Phys.: Condens. Matter* **11** 5661
[24] Mizoguchi T, Yoshiya M, Li J, Oba F, Tanaka I and Adachi H 2001 *Ultramicroscopy* **86** 363
[25] Mizoguchi T, Tanaka I, Mizuno M, Adachi H, Hashimoto T, Inui H and Yamaguchi M 2001 *Acta. Mater.* **49** 2321
[26] Filipponi A, Di Cocco A and Natoli C R 1995 *Phys. Rev.* B **52** 15122
[27] Rehr J J and Albers R C 2000 *Rev. Mod. Phys.* **72** 621
[28] Moreno M S, Jorissen K and Rehr J J 2007 *Micron* **38** 1
[29] Hatada K, Hayakawa K, Benfatto M and Natoli C R 2009 *J. Phys.: Condens. Matter* **21** 104206
[30] de Groot F M F 2005 *Coord. Chem. Rev.* **249** 31
[31] Ogasawara K, Iwata T, Koyama Y, Ishii I, Tanaka I and Adachi H 2001 *Phys. Rev.* B **64** 115413
[32] Ikeno H, Tanaka I, Miyamae T, Mishima T, Adachi H and Ogasawara K 2004 *Mater. Trans.* **45** 1414
[33] Ikeno H, Tanaka I, Koyama Y, Mizoguchi T and Ogasawara K 2005 *Phys. Rev.* B **72** 075123
[34] Ikeno H, Mizoguchi T, Koyama Y, Kumagai Y and Tanaka I 2006 *Ultramicroscopy* **106** 970
[35] Kumagai Y, Ikeno H, Oba F, Matsunaga M and Tanaka I 2008 *Phys. Rev.* B **77** 155124
[36] Ikeno H and Tanaka I 2008 *Phys. Rev.* B **77** 075127
[37] de Groot F M F and Kotani A 2008 *Core Level Spectroscopy of Solids Advances in Condensed Matter Science* (Boca Raton, FL: CRC Press)
[38] Ikeno H, de Groot F M, Stavitski E and Tanaka I 2009 *J. Phys.: Condens. Matter* **21** 104208
[39] Onida G, Reining L and Rubio A 2002 *Rev. Mod. Phys.* **74** 601
[40] Shirley E L 2000 *J. Electron Spectrosc. Relat. Phenom.* **110/111** 305
[41] Shirley E L 2004 *J. Electron Spectrosc. Relat. Phenom.* **136** 77
[42] Olovsson W, Tanaka I, Puschnig P, Ambrosch-Draxl C and Mizoguchi T 2009 *Phys. Rev.* B at press
[43] Olovsson W, Tanaka I, Puschnig P and Ambrosch-Draxl C 2009 *J. Phys.: Condens. Matter* **21** 104205
[44] Yamamoto T, Mizoguchi T and Tanaka I 2005 *Phys. Rev.* B **71** 245113
[45] Mizoguchi T, Tanaka I, Kunisu M, Yoshiya M, Adachi H and Ching W Y 2003 *Micron* **34** 249
[46] Kunisu M, Oba F, Ikeno H, Tanaka I and Yamamoto T 2005 *Appl. Phys. Lett.* **86** 121902
[47] Tatsumi K, Mizoguchi T, Yoshioka S, Yamamoto T, Suga T, Sekine T and Tanaka I 2005 *Phys. Rev.* B **71** 033202
[48] Yoshioka S, Oba F, Huang R, Tanaka I, Mizoguchi T and Yamamoto T 2008 *J. Appl. Phys.* **103** 014309
[49] Mizoguchi T, Seko A, Yoshiya M, Yoshida H, Yoshida T, Ching W Y and Tanaka I 2007 *Phys. Rev.* B **76** 195125
[50] Blaha P, Schwarz K, Madsen G, Kvasicka D and Luitz J 2001 *WIEN2k, An Augmented Plane Wave + Local Orbitals Program for Calculating Crystal Properties* Vienna, TU Wien
[51] Rez P and Muller D A 2008 *Annu. Rev. Mater. Res.* **38** 535
[52] Ching W Y 1990 *J. Am. Ceram. Soc.* **73** 3135
[53] Kunisu M, Tanaka I, Yamamoto T, Suga T and Mizoguchi T 2004 *J. Phys.: Condens. Matter* **16** 3801
[54] Guo J H, Vayssieres L, Persson C, Ahuja R, Johansson B and Nordgren J 2002 *J. Phys.: Condens. Matter* **14** 6969
[55] Suga T, Kameyama S, Yoshioka S, Yamamoto T, Tanaka I and Mizoguchi T 2005 *Appl. Phys. Lett.* **86** 163113
[56] Hamann D R and Muller D A 2002 *Phys. Rev. Lett.* **89** 126404
[57] Kimoto K, Matsui Y, Nabatame T, Yasuda T, Mizoguchi T, Tanaka I and Toriumi A 2003 *Appl. Phys. Lett.* **83** 4306
[58] Bouchet D and Colliex C 2003 *Ultramicroscopy* **96** 139
[59] Nakahira A, Okajima T, Honma T, Yoshioka S and Tanaka I 2006 *Chem. Lett.* **35** 856
[60] Botton G A, Guo G Y, Temmerman W M and Humphreys C J 1996 *Phys. Rev.* B **54** 1682
[61] Muller D A, Singh D J and Silcox J 1998 *Phys. Rev.* B **57** 8181
[62] Krause M O and Oliver J H 1979 *J. Phys. Chem. Ref. Data* **8** 329
[63] Fuggle J C and Alvarado S F 1980 *Phys. Rev.* A **22** 1615